Electronic Supplementary Material (ESI) for ChemComm.

A Bowl-Shaped Phosphangulenes Protected Cubic Cu_{58} Nanocluster

Qian Zhang#[1], Hao Zheng#[1], Jie Zhou#[1], Jia-Ji Yang[1], Kai-Yue Xu[1], Lian-Yun Shen[1], Zong-Jie Guan[2] and Yang Yang*[1]

1 School of Chemistry and Materials Science, Jiangsu Normal University, Xuzhou 221116, China.

E-mail: yangyang@jsnu.edu.cn;

2 College of Chemistry and Chemical Engineering, Hunan University, Changsha, 410082, China.

#These authors contribute equally.

Contents:

I. Physical measurements

UV-Vis spectra were measured using a Shimadzu 2550 spectrometer. NMR data were acquired using a Bruker Avance II spectrometer operating at frequencies of 400 MHz. Mass spectra were obtained using Bruker Impact II high-definition spectrometers with electrospray ionization time-of-flight (ESI-TOF) technique. X-ray photoelectron spectroscopy (XPS) measurements were performed using a Thermo Fisher K-Alpha spectrometer. IR spectra were recorded using a Thermo Fisher Scientific Nicolet Is10 spectrometer. Energy-dispersive X-ray spectroscopy (EDS) and the scanning electron microscopy (SEM) characterizations were done by Hitachi SU-8100. Gas chromatography was performed on a GC-7900 gas chromatograph. Electrochemistry was done with electrochemical workstation chi760e.

II. Synthesis

All reagents employed were commercially available and were used without further purification. The solvents used were of analytical grade. Phosphangulene (simplified as phang) was synthesized according to a reported literature.[1]

Synthesis of ***Cu$_{58}$***. Under a nitrogen atmosphere, 500 mg of the phang ligand was dissolved in a mixture of 25 mL of CH_2Cl_2 and 5 mL of CH_3OH. Then, 413.9 mg of $[Cu(CH_3CN)_4]BF_4$ was added and stirred for one hour. Afterward, 123.4 μL of PETH (dissolved in 4 mL of CH_2Cl_2) was added to the above solution and stirred for 20 minutes. Following this, a freshly prepared solution of 34.8 mg $NaBH_4$ (dissolved in 2 mL of ethanol) was gradually added, resulting in a gradual color change to deep red. The mixture was stirred for 4 hours and then the solvent was removed by rotary evaporation. The resulting solid was dissolved in 15 mL of CH_2Cl_2, yielding a deep red solution. The solution was filtered into a long-thin tube, and a sufficient amount of diethyl ether was slowly layered onto the solution in the tube. After 4 days storing at 4°C, dark red cubic crystals, referred to as **Cu$_{58}$** clusters, were obtained in a 10% yield (based on copper). The synthesis of **Cu$_{58}$**-D clusters was identical to Cu_{58} clusters, except that $NaBD_4$ was used instead of $NaBH_4$. ESI-MS: cal. $[Cu_{58}(phang)_4(PET)_{36}(H)_{20}]^{2+}$ m/z = 4931.35, found m/z = 4931.27. XPS (binding energy, eV): Cu $2p^{3/2}$ = 932.8, Cu $2p^{1/2}$ = 952.6.

*Cluster-to-Cluster transformation for PPh$_3$-****Cu$_{58}$***

10 mg crystals of **Cu_{58}** were dissolved in 5 mL CH_2Cl_2. 10.5 mg (10 eq.) triphenylphosphine was added into the solution and the mixture was stirred for 24 hours. The solution was concentrated before the addition of diethyl ether to precipitate the products of PPh_3-**Cu_{58}**. ESI-MS: cal. $[Cu_{58}(PPh_3)_4(PET)_{36}(H)_{20}]^{2+}$ m/z = 4847.47, found m/z = 4847.53.

III. Photocurrent response

3 mg of **Cu_{58}** solid/ 3 mg C_{60} powder / 1.5 mg **Cu_{58}** together with 1.5 mg C_{60} were suspended in a mixture of 200 μL ethanol and 10 μL naphthol (**Cu_{58}** and C_{60} can partially dissolve in ethanol and naphthol to form a homogeneous mixture), respectively. The suspensions were sonicated for 15 min before dropping onto a conductive glass substrate (indium-doped SnO_2) and dried. The indium-doped SnO_2 (ITO) was the working electrode. The photocurrent experiments were carried out in the standard phosphate buffer solution with the pH of 6.8 under the illumination of Xe lamp (300W, distance to sample: 18 cm). The data was collected using an electrochemical workstation chi760e and analyzed using the chi760e software.

IV. Photo-driven hydrogen liberations

The photo-driven hydrogen liberation reaction was carried out in a gas-closed system with a reactor made of quartz. A blue LED lamp was used as a light source. The distance between the lamp and the reactor is 7cm. In a typical experiment, **Cu_{58}**-C_{60} adduct (13 mg, which was prepared by sonicating 10 mg **Cu_{58}** and 3 mg C_{60} in 15 mL dichloromethane for 15 min to form a clear solution and further evaporating the solvent to obtain solid) for tube A, the crystals of **Cu_{58}** (10 mg) for tube B, the C_{60} powder (7 mg) for tube C, were added in an aqueous solution (4 mL) containing triethanolamine (TEOA, 1.6 ml) respectively. The mixtures were sonicated for 15 min to form homogeneous suspensions. Then, the suspensions were irradiated for 8 hours. The amount of hydrogen produced was measured with a gas chromatograph (GC-7900, China, molecular sieve 5A, TCD) using N_2 as the carrier gas.

V. X-ray crystallography

We conducted diffraction experiments at 100 K using Cu Kα (λ = 1.54184 Å) X-ray sources and a Rigaku “XtaLAB Synergy, Dualflex, HyPix” X-ray diffractometer. The crystals were fragile and

easily lost solvent molecules. Thus, rapid handling of the samples was needed. Despite these measures and several trials, few reflections at greater than 0.99 Å resolution were observed and the data were collected to this limit. Furthermore, there was a significant drop-off in diffraction intensity after around 1.25 Å resolution resulting in a low ratio of observed/unique reflections. Nevertheless, the quality of the data is far more than sufficient to establish the connectivity of the structure. The obtained diffraction data were processed for reduction and cell refinement using the *CrysAlisPro* (1.171.42.72a Version, Rigaku Oxford Diffraction, 2022). Multi-scan absorption corrections were applied. The structures were solved using the *ShelXT* structure solution program in *OLEX2*,[2] employing intrinsic phasing, and refined using the *ShelXL* refinement package with least-squares minimization. Due to the limited resolution of the data and high levels of thermal motion throughout the structure, the refinements of Cu, S and P were done anisotropically, while those of H, C, and O were done isotropically. Substantial restraints were required in order to obtain a reasonable model for the organic parts of the structure. The hydrogen atoms of organic ligands were generated geometrically. To ensure charge balance, the correct chemical formula of **Cu_{58}** reported in the CIF considered the undefined counterions and hydrides that determined by ESI-MS into consideration. The *SQUEEZE* routines in *PLATON* were utilized during the structural refinements to eliminate any undefined solvents.[3] Detailed crystallographic data is provided in Table S1.

CheckCIF gives 8 A and 10 B level alerts, mostly resulting from the limited resolution of the data (High wR2 Value, low sine(theta_max)/wavelength, low bond precision, high/low Ueq of some atoms) and isotropic modelling of organic ligands. Four alerts (A level) relating to the "Isolated Metal Atom found in Structure" is due the intrinsic features of the structure with copper ions in the cluster center supporting by solely metal-metal bonds. Four alerts (B level) relating to short contacts of phenyl protons with those of the neighbours appear to be intrinsic features of the structure although it should be noted that there is some uncertainty in the position of the phenyl protons due to thermal motion of these rings.

VI. Calculations

Density functional theory (DFT) calculations were conducted using the quantum chemistry program Gaussian 16,[4] employing the 6-31G* basis set for all elements.[5] Structural optimizations were carried out at the B3LYP/6-31G* level, utilizing the crystal structure of cluster **Cu_{58}** as a basis with

PET^- and phangs ligands being simplified into HS^- and PH_3. The initial hydride positions were proposed on the basis of previous reports including the half cubic Cu_{36}[6] and the Ag_{40}[7] possessing a cubic Ag_8 core with twelve hydrides residing on its twelve edges. When optimizing the position of hydride, the rest parts were frozen. Then full optimization was done while heavy atoms Cu and S were not allowed to optimized. Time-dependent DFT calculations were conducted using the CAM-B3LYP function. One hundred singlet states (nstates=100, singlet) were chosen in the calculations. Orbital composition analysis with Mulliken partition and calculation of absorption spectra were carried out using Multiwfn.[8]

VII. Supporting table

Table S1. Crystallographic Data and Structure Refinement for Cu_{58}.

	Cu_{58}
Formula	$Cu_{58}P_4S_{36}C_{360}H_{380}O_{12}B_2F_8$
Formula weight	10035.60
Crystal system	Tetragonal
Space group	*I*41/acd
a [Å]	50.9312(3)
b [Å]	50.9312(3)
c [Å]	64.4799(7)
α [°]	90
β [°]	90
γ [°]	90
V [Å^3]	167260(3)
Z	16
T [K]	100
F (000)	80576
Crystal size (mm^3)	0.06*0.05*0.05
ρ_{calcd} (g/cm^3)	1.594
μ (mm^{-1})	5.281 [a]

R_{int}	0.0424
R_1, wR_2 ($I \geq 2\sigma$ (I))	0.1516 0.4693
R_1, wR_2 (all data)	0.1647 0.4847
CCDC No.	2310083

[a]Cu Kα radiation.

VIII. Supporting figures

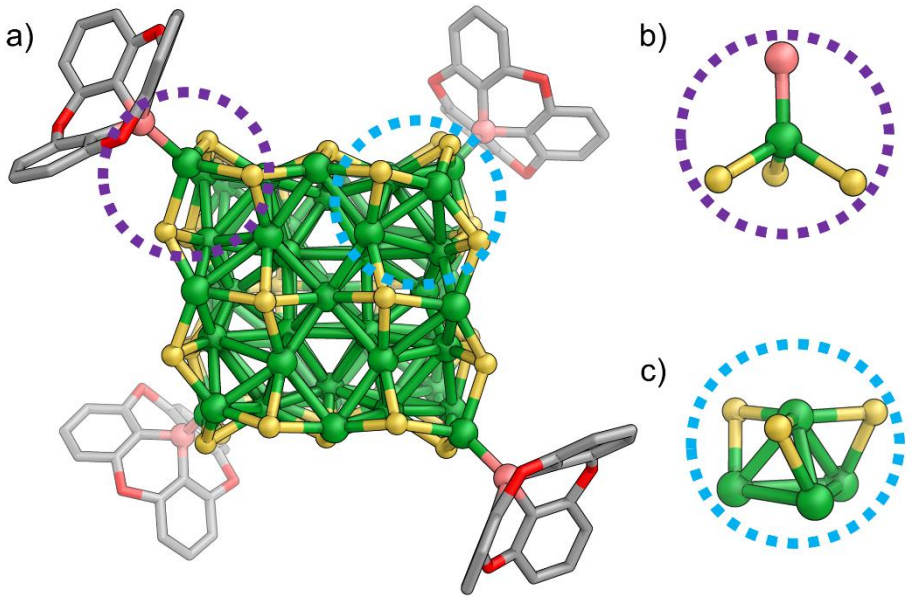

Fig. S1. a) The core structure of **Cu_{58}**; b) the vertex with phang ligated having a PS_3 in a tetrahedron configuration with the Cu ion in the center; b) the vertex without phang ligated having a Cu ion coplanar to the S_3 triangles.

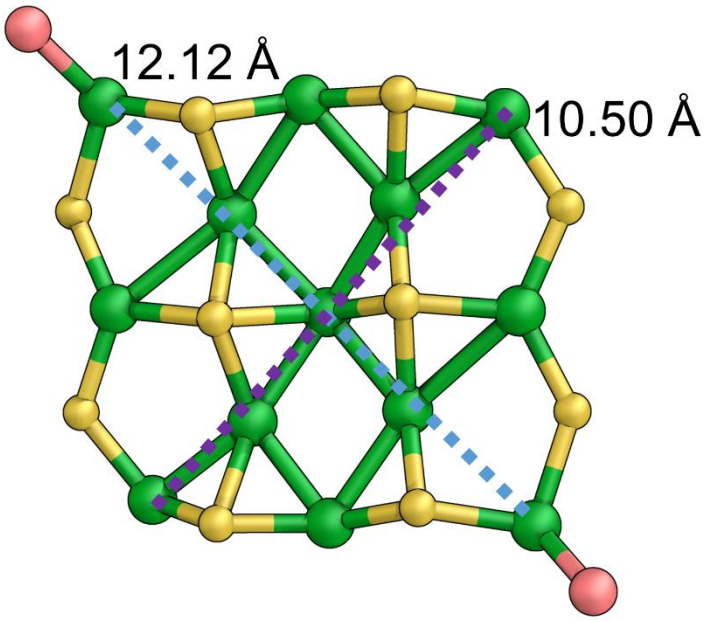

Fig. S2. One cubic facet in a rhombus shape with the long and short diagonals being 12.12 Å and 10.50 Å, respectively.

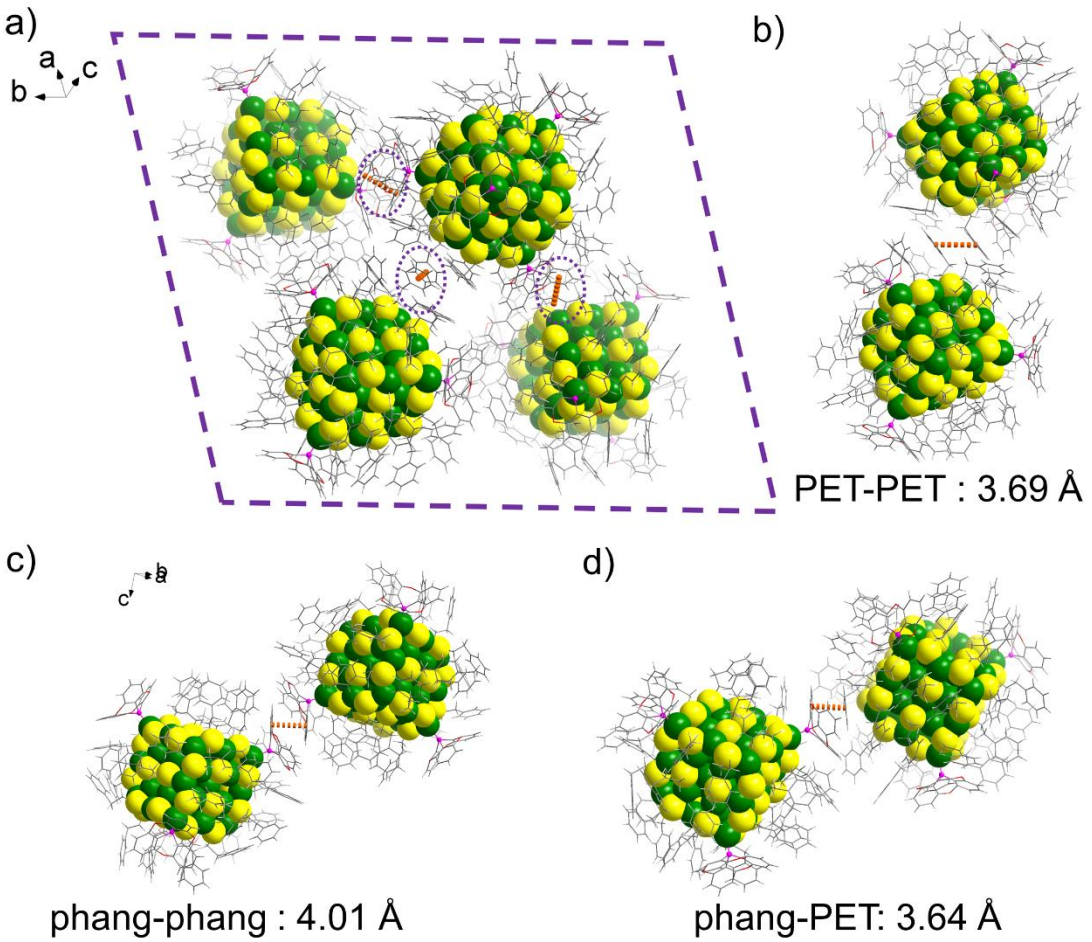

Fig. S3. a) clusters of **Cu_{58}** packing in the unit cell; b) neighboring clusters with the PET-PET π-π interaction c) neighboring clusters with the phang-phang π-π interaction; d) neighboring clusters with the phang-PET π-π interaction.

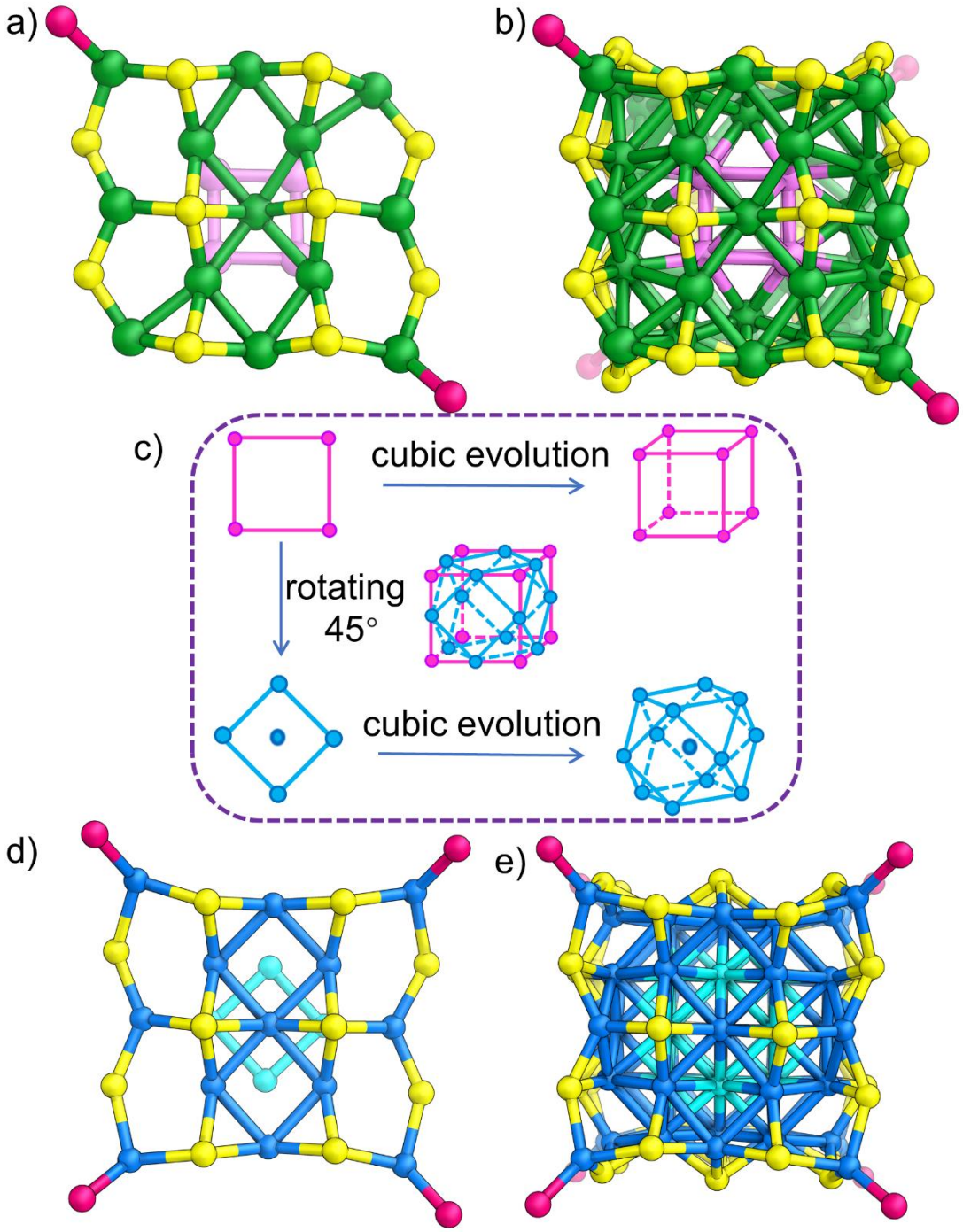

Fig. S4. a) the repeating unit of **Cu_{58}**; b) the core-shell of **Cu_{58}** with the core highlighting in pink; c) the cubic evolution of repeating units leading to the difference in the core structure of **Cu_{58}** and Ag_{63}; d) the repeating unit of the core of Ag_{63}; e) the core-shell of structure of Ag_{63} with the core highlighting in light-blue.

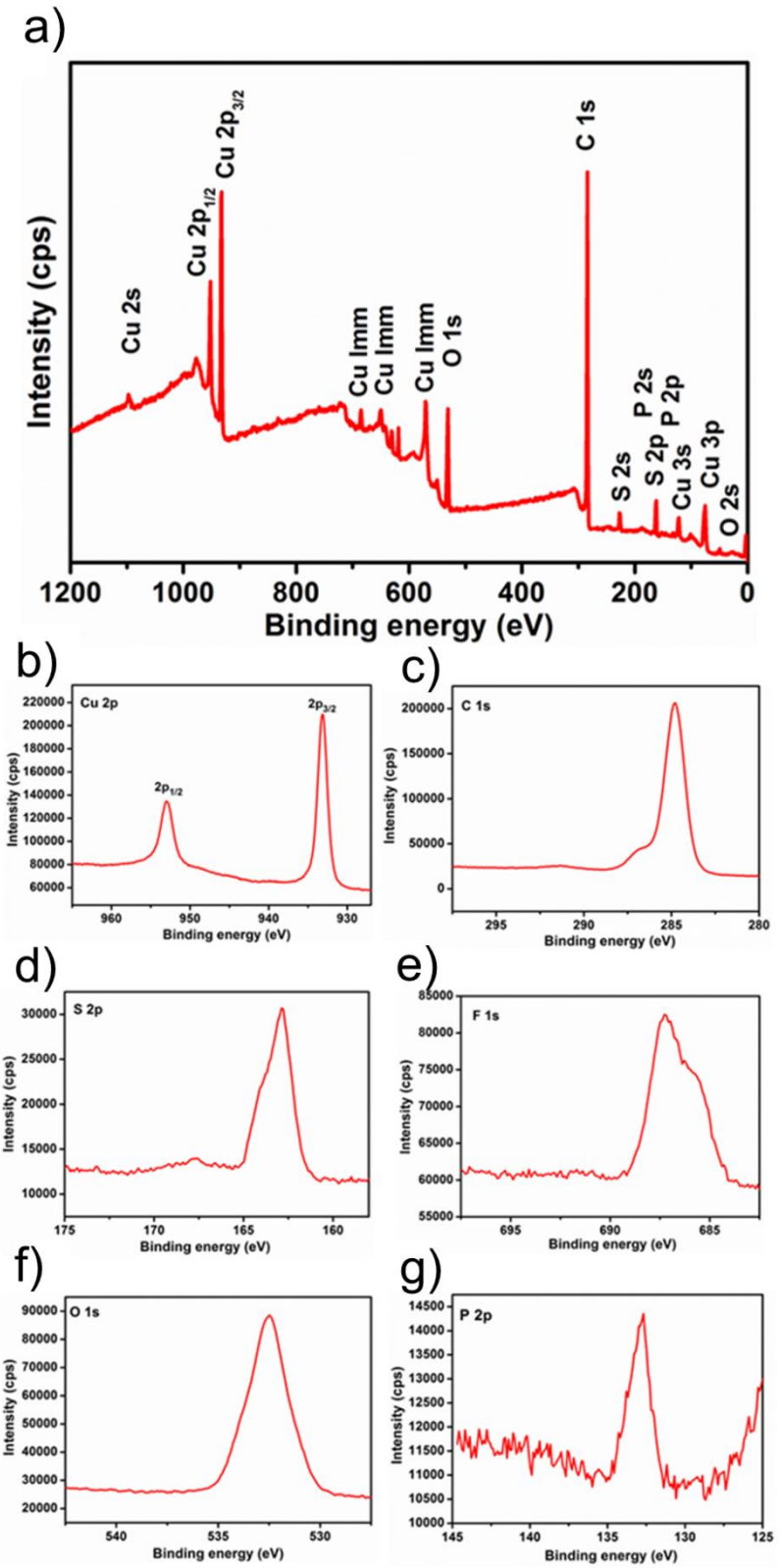

Fig. S5. a) The full XPS spectrum of **Cu_{58}**; high-resolution XPS spectra of b-g) Cu 2p, C 1s, S 2p, F 1s, O 1s and S 2p.

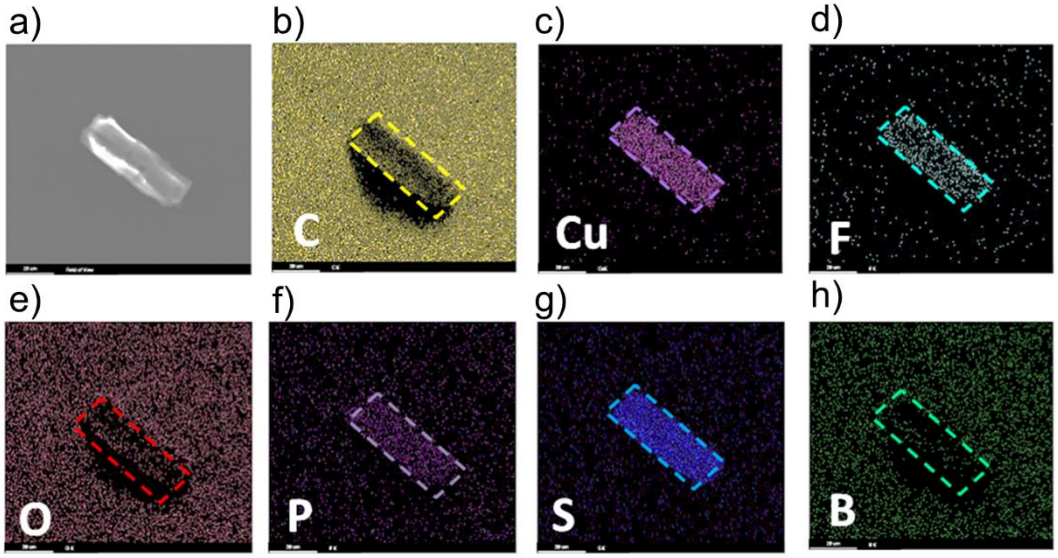

Fig. S6. a) Scanning electron microscope (SEM) image of a crystal of **Cu_{58}**, b-h) energy dispersive spectrometry (EDS) mapping of C, Cu, F, O, P, S and B.

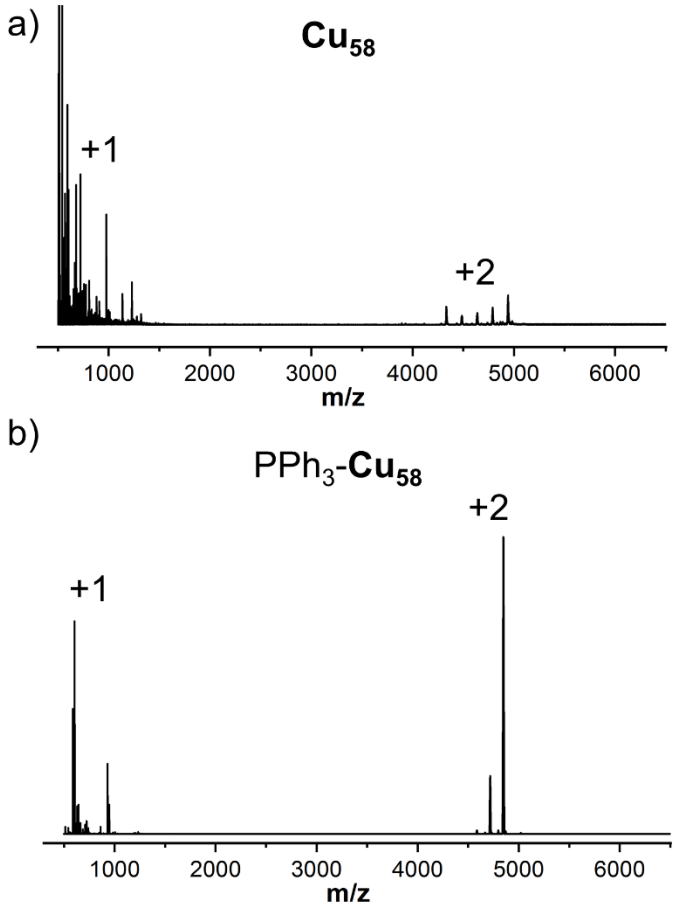

Fig. S7. The positive mode of full range ESI-MS spectra of a) **Cu_{58}** and b) PPh_3-**Cu_{58}** in dichloromethane. Peaks below 1500 Da are +1 charged fragments.

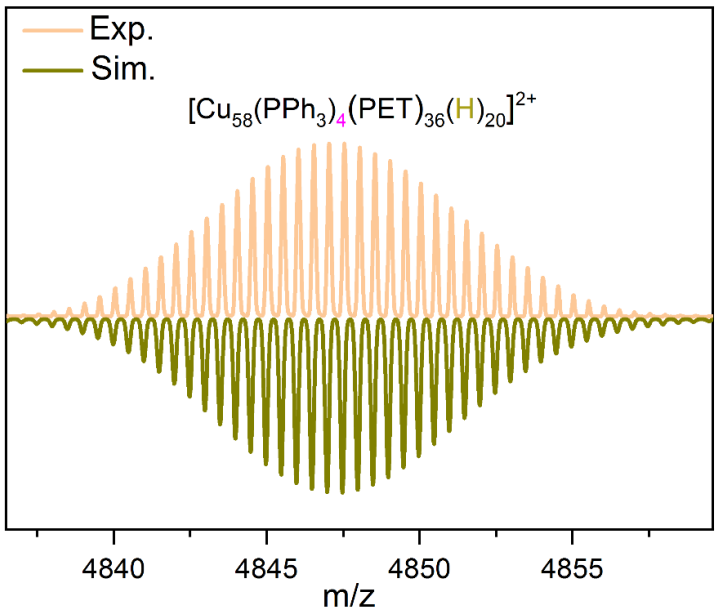

Fig. S8. The comparison of experimental and simulated isotope patterns of molecular peak of $[Cu_{58}(PPh_3)_4(PET)_{36}(H)_{20}]^{2+}$.

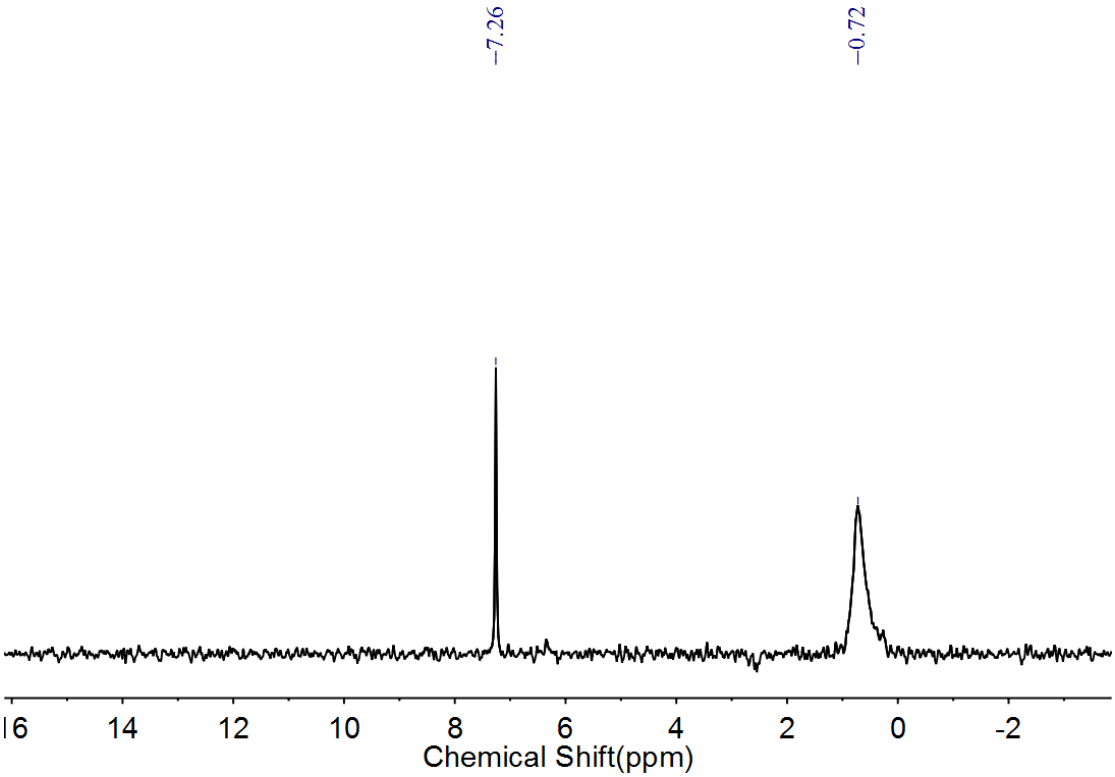

Fig. S9. ^{2}H NMR spectrum (600 MHz, 298 K) of **Cu_{58}-D** in chloroform. The peak at 7.26 ppm is the chloroform solvent.

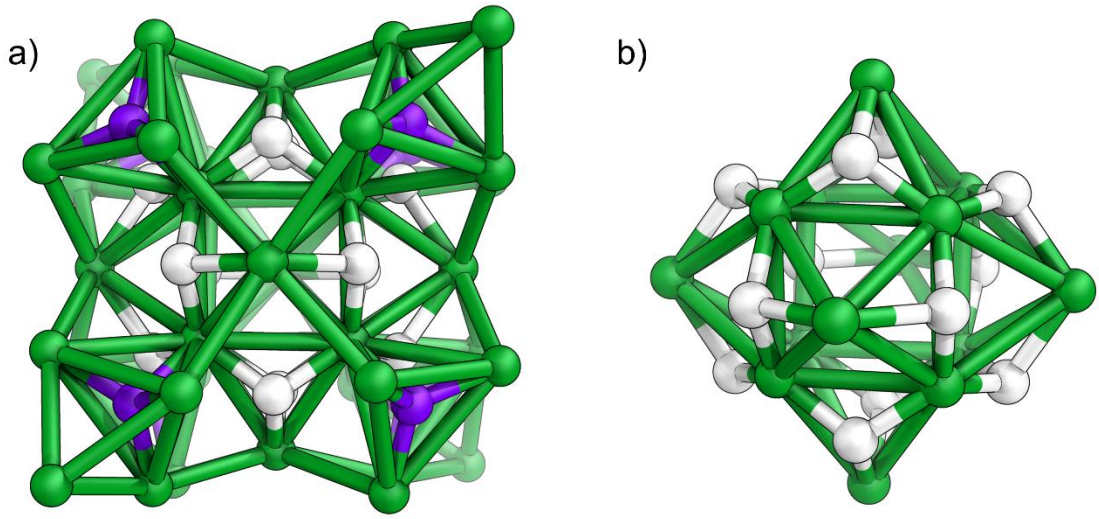

Fig. S10. a) The twenty hydrides calculated by DFT highlighting in white (in μ_3 mode) and purple (in μ_4 mode), b) twelve hydrides in a μ_3 mode that symmetrical located on the triangular surfaces of the capped-cube.

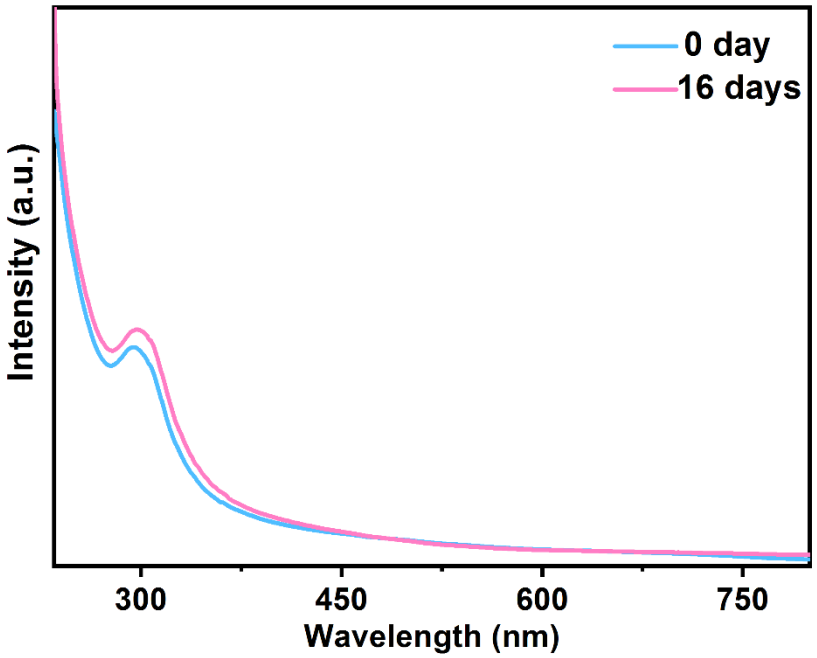

Fig. S11. The UV-vis absorption spectra of **Cu_{58}** in tetrahydrofuran (1.3×10^{-5} M) and the solution kept after 16 days.

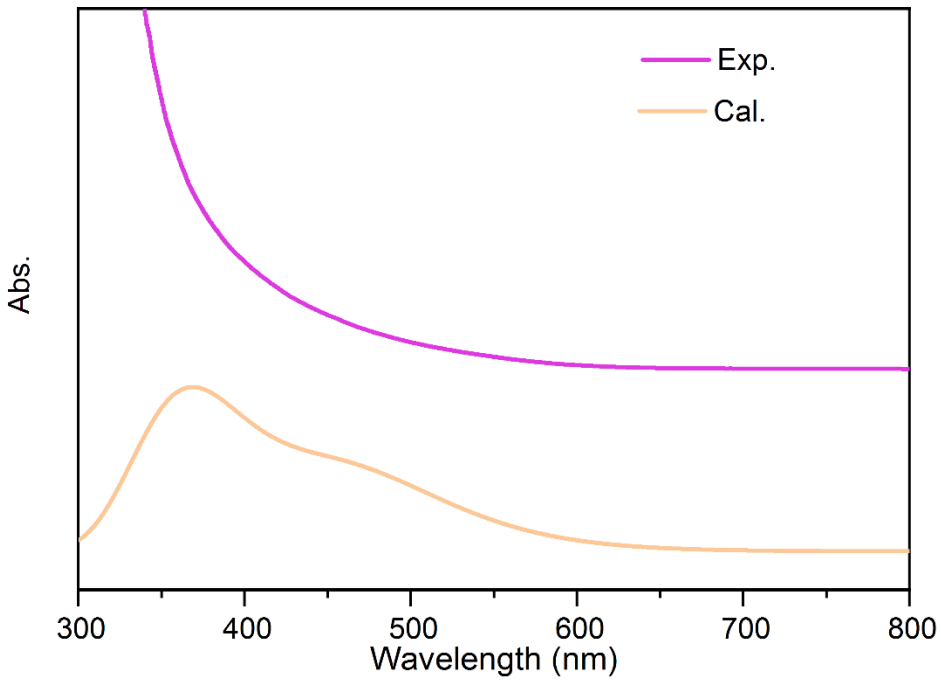

Fig. S12. The comparison of the experimental absorption spectrum of **Cu_{58}** in dichloromethane and the calculated one.

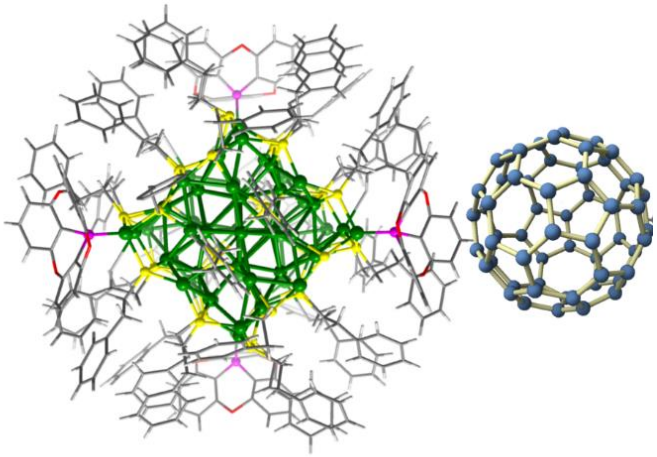

Fig. S13. The proposed schematic diagram of the interactions of **Cu_{58}** and C_{60} due to the geometric complementation of the curved phang ligand and curved surface C_{60}.

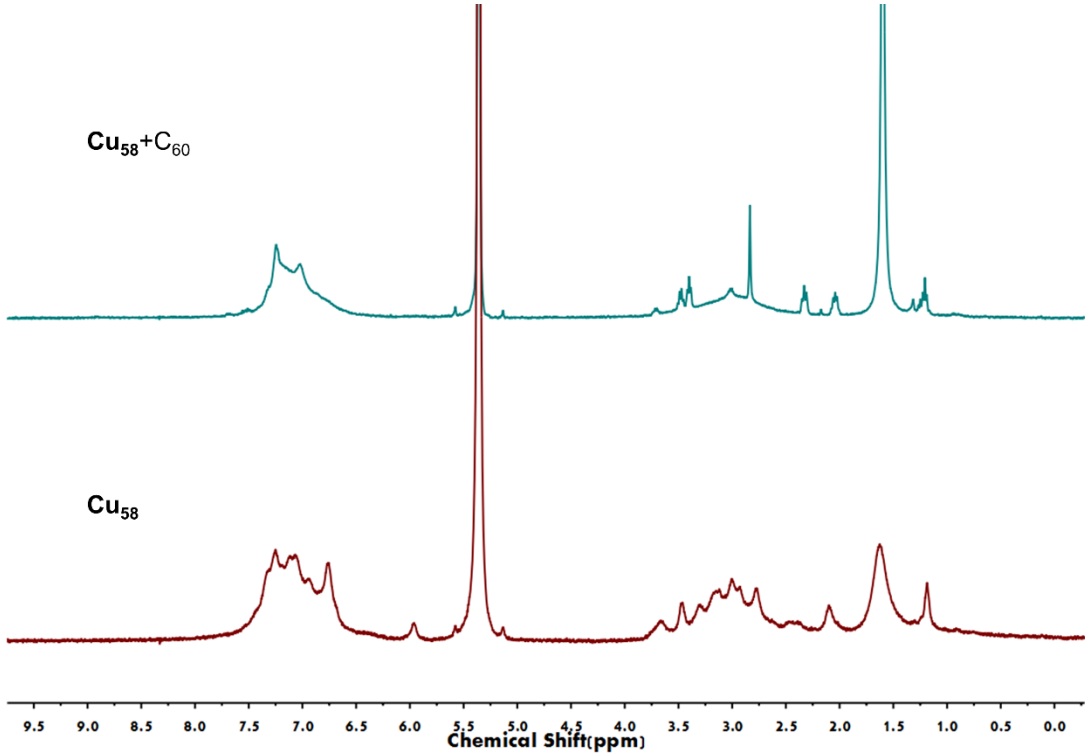

Fig. S14. ^{1}H NMR spectra (400 MHz, 298 K) of **Cu$_{58}$** in CD_2Cl_2 (bottom) and after the addition of 4 eq. C_{60} dissolved in CS_2 (top). The spectrum showed significant differences in the phenyl range of 6.5-8.0 ppm upon the addition of C_{60} compared to that of **Cu$_{58}$**, suggesting interactions between **Cu$_{58}$** and C_{60}.

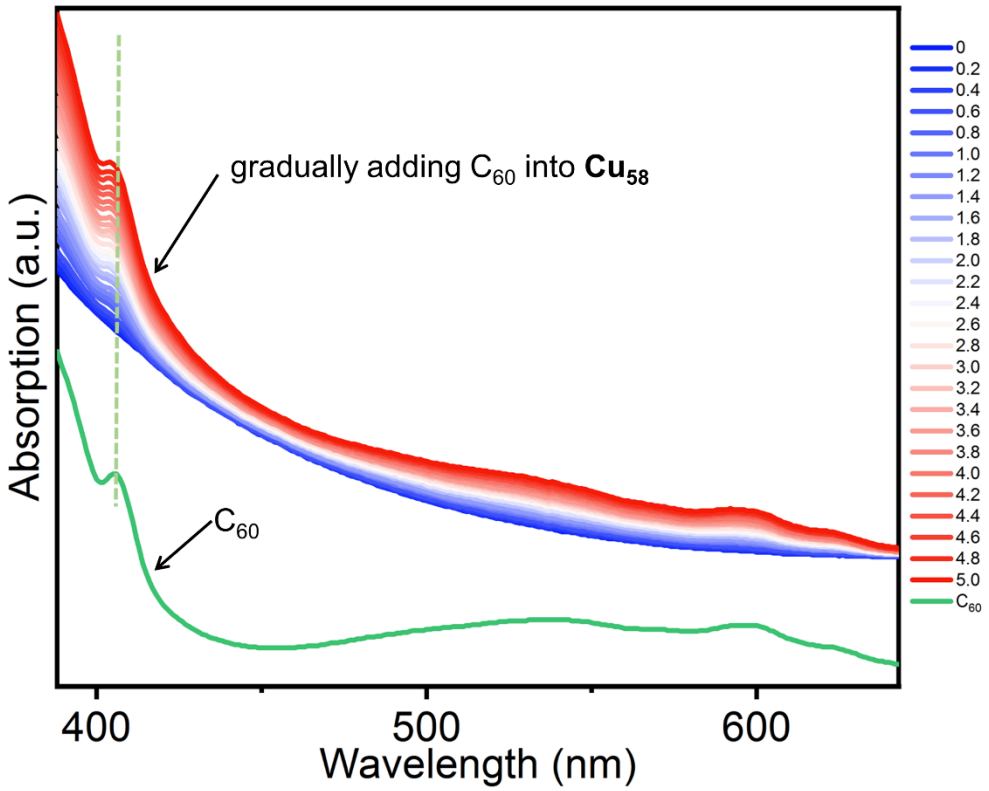

Fig. S15. The absorption spectra of **Cu_{58}** in dichloromethane with the gradual addition of C_{60} dissolved in dichloromethane. Comparing with the same amount pure C_{60} dissolved in the same solution, the characteristic peak of C_{60} at 406 nm obviously shifted, indicating interactions between **Cu_{58}** and C_{60}.

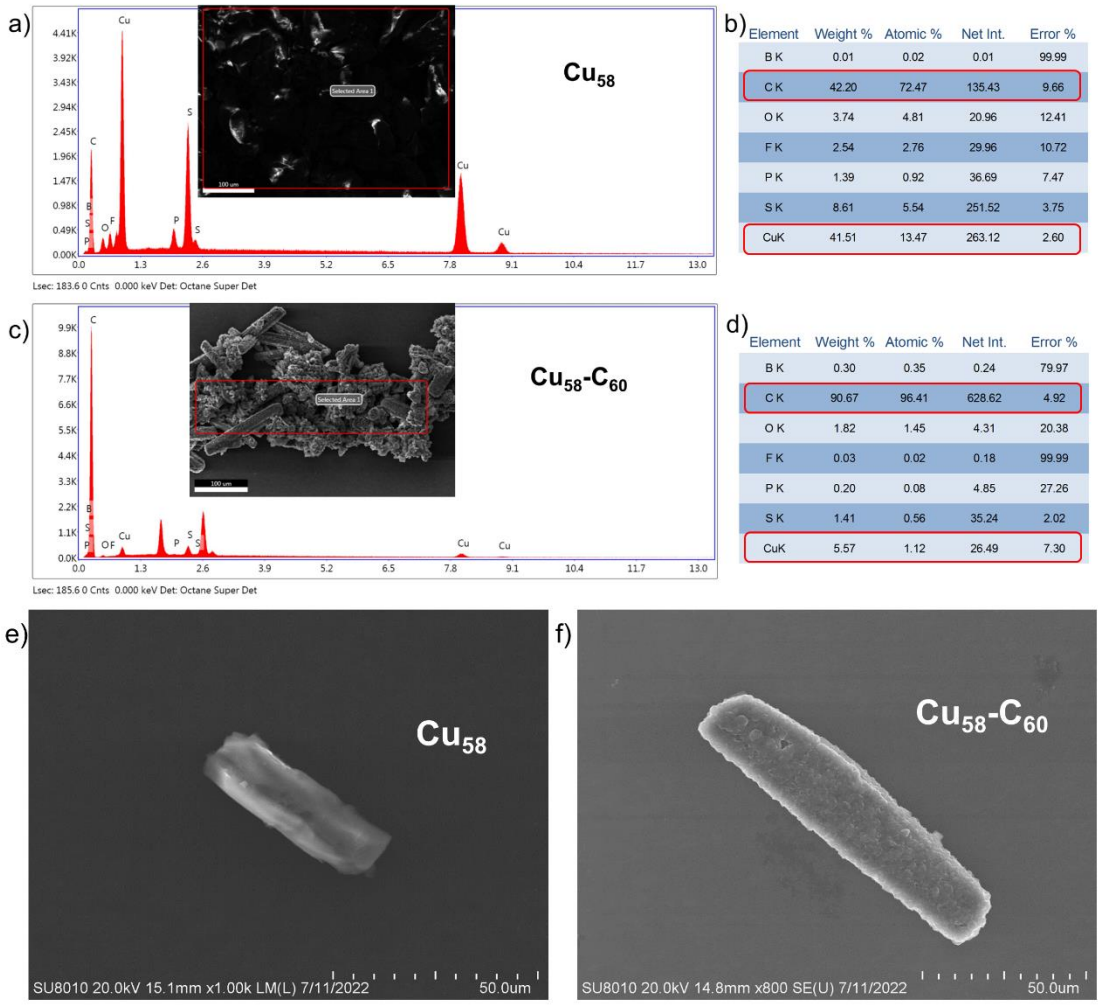

Fig. S16 a) The eds spectrum of **Cu_{58}** crystals; b) the corresponding semiquantitative element amounts; c) The eds spectrum of **Cu_{58}**-C_{60} adduct, which was prepareD by evaporating a CH_2Cl_2 solution dissolving **Cu_{58}** with 4 eq. C_{60}; d) the corresponding semiquantitative element amounts; e) high resolution SEM image of crystal of **Cu_{58}**; f) high resolution SEM image of **Cu_{58}**-C_{60}. The **Cu_{58}**-C_{60} shows higher amount of C and lower amount of Cu, in line with the expectation of mixing **Cu_{58}** with C_{60}. The SEM images in **Fig. S16c** and **Fig. S16f** show that the surfaces of samples of **Cu_{58}**-C_{60} are rough compared to that of **Cu_{58}**, indicate that C_{60} solid may closely attach onto the aggregation of **Cu_{58}** solids to form a relative homogeneous solid mixture.

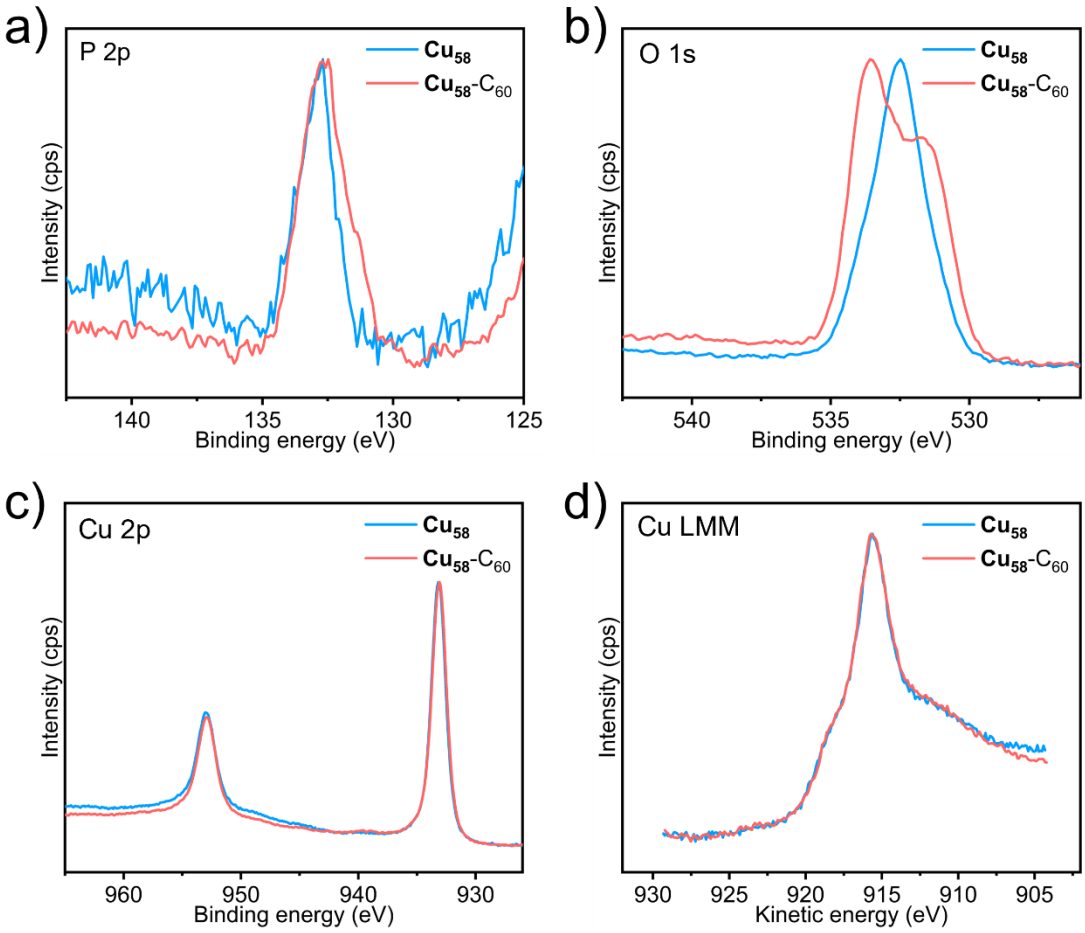

Fig. S17. Comparisons of high-resolution XPS spectra of **Cu_{58}** and mixture adduct of **Cu_{58}**-C_{60} (which was prepared by evaporating a CH_2Cl_2 solution dissolving **Cu_{58}** with 4 eq. C_{60}): a) P 2p; b) O 1s; c) Cu 2p; d) Cu LMM. The P and O element of **Cu_{58}-C_{60}** are obviously different from those of **Cu_{58}**, while the Cu element is very similar, indicating there are interactions between **Cu_{58}** and C_{60} through the phosphangulene ligand (which contain the P and O elements).

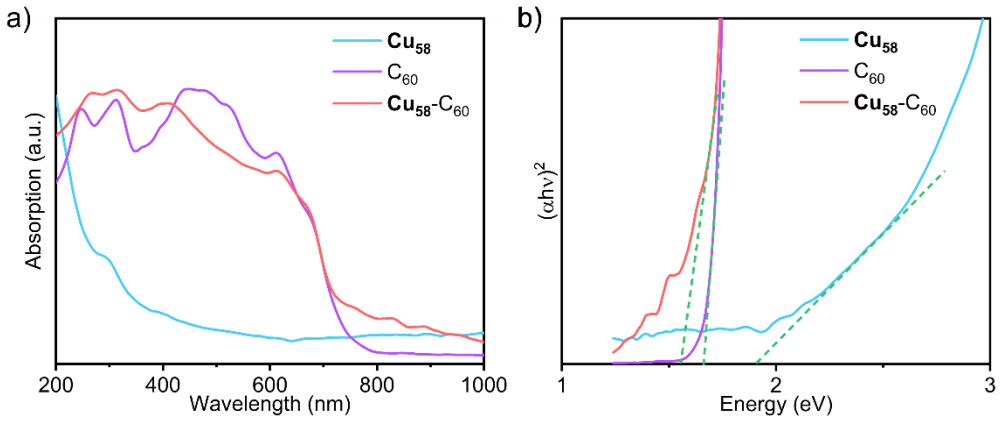

Fig. S18 a) The solid state UV-Vis-NIR absorption spectra (diffuse reflectance mode) of **Cu$_{58}$**-C$_{60}$, which was prepared by evaporating a CH_2Cl_2 solution dissolving **Cu$_{58}$** with 4 eq. C$_{60}$; **Cu$_{58}$** and C$_{60}$, b) the corresponding energy band-gaps. **Cu$_{58}$**-C$_{60}$ is different from that of both individual pristine states and simple sum of individuals, verifying interactions between **Cu$_{58}$** and C$_{60}$. **Cu$_{58}$**-C$_{60}$ has smaller band-gap than **Cu$_{58}$** and C$_{60}$. The photogenerated electron-hole pairs are produced due to irradiation with light sources and absorption of the samples (transitions of electrons from HOMO and LUMO), which further drift in opposite directions when connected to the circuit resulting in photocurrents.[9]

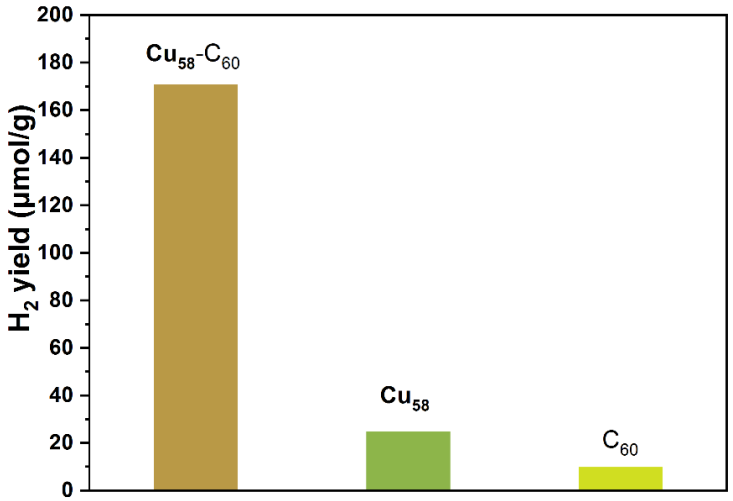

Fig. S19. Photo-driven hydrogen liberations of **Cu$_{58}$**-C$_{60}$, pristine **Cu$_{58}$** and pristine C$_{60}$. 10 equivalents hydrogen per cluster will be liberated, if all the hydrides were converted into hydrogen gas. The theoretical value will be 498.5 μmol/g for 10 mg **Cu$_{58}$**. Pure **Cu$_{58}$** produced 25 μmol/g H_2 gas. In the control experiment, very small amount of hydrogen gas was produced by C_{60}, which may be due to its semiconductor properties[10]. The light-driven electron-hole separation makes the excited **Cu$_{58}$** not stable in H_2O environment and the hydrides (H^-) tend to combine with H^+ in water leading the transformation from **Cu$_{58}$** into other small Cu(I) species with concomitant H_2 evolution. A previous report by C. W. Liu and co-worker[11] demonstrated that $[Cu_{20}H_{11}(S_2P(O^iPr)_2)_9]$ can convert into smaller $[Cu_7H\{S_2P(O^iPr)_2\}_6]$ (Cu in +1 charged state) after H_2 release. Further supports regarding the resultant are shown in **Fig. S20** and **S21**.

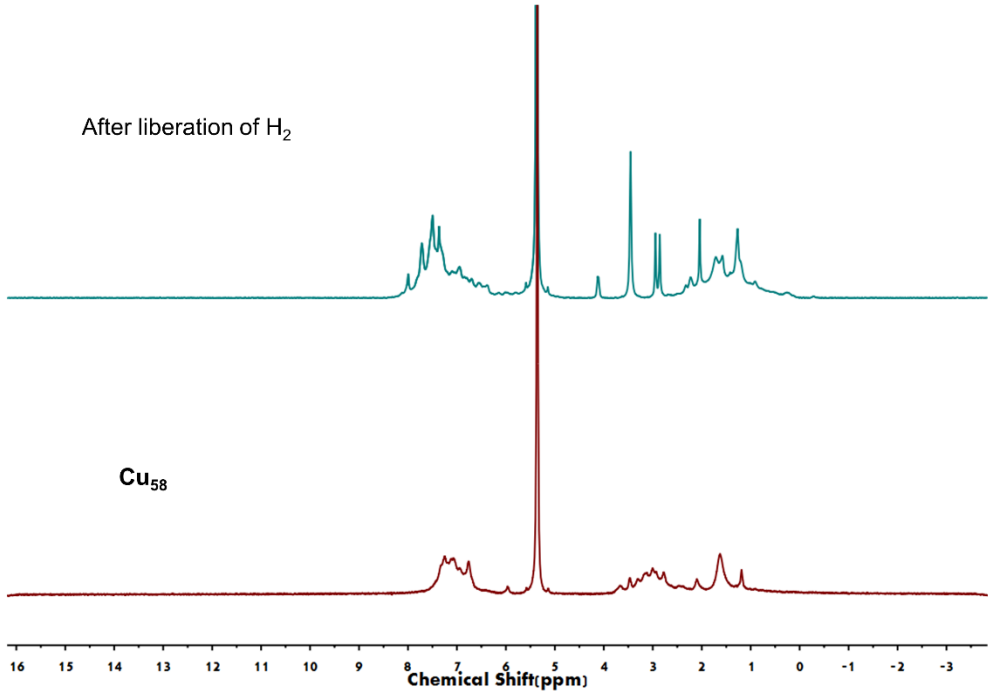

Fig. S20. The comparison of ^{1}H NMR spectra (400 MHz, 298 K) of **Cu_{58}** in CD_2Cl_2 (bottom) with the one after the photo-driven hydrogen liberation. The spectra indicated that **Cu_{58}** transformed into other species, which were not Cu(II) ones.

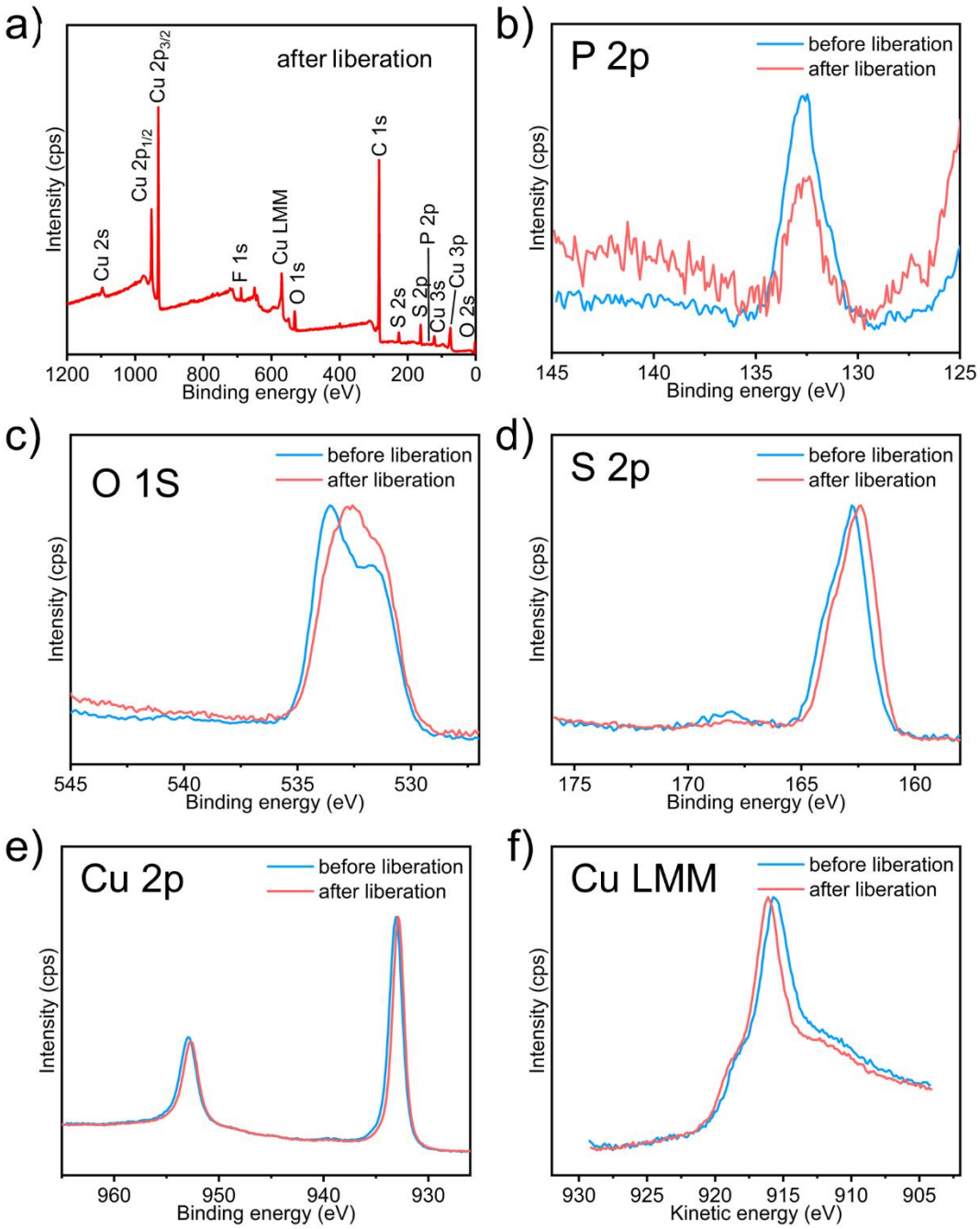

Fig. S21. a) The full XPS spectrum of **Cu$_{58}$**-C_{60} (which was prepared by evaporating a CH_2Cl_2 solution dissolving **Cu$_{58}$** with 4 eq. C_{60}) after the photo-driven hydrogen liberation; comparisons of high-resolution XPS spectra of b-g) P 2p, O 1s, S 2p, Cu 2p, and Cu LMM with the one before the liberation. The XPS of the resultant after liberation of H_2 showed that the Cu of it in +1 charged state but with a slightly difference compared to **Cu$_{58}$**. This indicated the photo-exited **Cu$_{58}$** decomposed to other Cu(I) species with concomitant H_2 evolution.

References:

1. F. C. Krebs, P. S. Larsen, J. Larsen, C. S. Jacobsen, C. Boutton and N. Thorup, *J. Am. Chem. Soc.*, 1997, **119**, 1208.
2. (a) G. Sheldrick, *Acta Crystallogr., Sect. A*, 2015, **71**, 3; (b) O. V. Dolomanov, L. J. Bourhis, R. J. Gildea, J. A. K. Howard and H. Puschmann, *J. Appl. Crystallogr.*, 2009, **42**, 339.
3. A. L. Spek, *Acta Crystallogr C Struct Chem*, 2015, **71**, 9.
4. M. J. Frisch, G. W. Trucks, H. B. Schlegel, G. E. Scuseria, M. A. Robb, J. R. Cheeseman, G. Scalmani, V. Barone, G. A. Petersson, H. Nakatsuji, X. Li, M. Caricato, A. V. Marenich, J. Bloino, B. G. Janesko, R. Gomperts, B. Mennucci, H. P. Hratchian, J. V. Ortiz, A. F. Izmaylov and a. et., *Gaussian 16*, Gaussian Inc.: Wallingford.
5. (a) P. J. Hay and W. R. Wadt, *J. Chem. Phy.*, 1985, **82**, 299; (b) W. J. Hehre, R. Ditchfield and J. A. Pople, *J. Chem. Phy.*, 1972, **56**, 2257.
6. C. Dong, R.-W. Huang, C. Chen, J. Chen, S. Nematulloev, X. Guo, A. Ghosh, B. Alamer, M. N. Hedhili, T. T. Isimjan, Y. Han, O. F. Mohammed and O. M. Bakr, *J. Am. Chem. Soc.*, 2021, **143**, 11026.
7. X. Yuan, C. Sun, X. Li, S. Malola, B. K. Teo, H. Häkkinen, L.-S. Zheng and N. Zheng, *J. Am. Chem. Soc.*, 2019, **141**, 11905.
8. T. Lu and F. Chen, *J. Comput. Chem.*, 2012, **33**, 580.
9. A. K. Das, S. Biswas, V. S. Wani, A. S. Nair, B. Pathak and S. Mandal, *Chem. Sci.*, 2022, **13**, 7616.
10. Y. Pan, X. Liu, W. Zhang, Z. Liu, G. Zeng, B. Shao, Q. Liang, Q. He, X. Yuan, D. Huang and M. Chen, *Applied Catalysis B: Environmental*, 2020, **265**, 118579.
11. R. S. Dhayal, J.-H. Liao, Y.-R. Lin, P.-K. Liao, S. Kahlal, J.-Y. Saillard and C. W. Liu, *J. Am. Chem. Soc.*, 2013, **135**, 4704.